Physico-chemical properties of WO_3/TiO_2 systems employed for 4-nitrophenol photodegradation in aqueous medium

C. Martín, G. Solana and V. Rives*

Departamento de Química Inorgánica, Universidad de Salamanca, Salamanca, Spain

G. Marcì, L. Palmisano and A. Sclafani

Dipartimento di Ingegneria Chimica dei Processi e dei Materiali, Università di Palermo, Viale delle Scienze, 90128 Palermo, Italy

Received 11 July 1997; accepted 21 October 1997

A series of polycrystalline WO_x/TiO_2 samples were prepared by means of a conventional impregnation method. The samples were characterized by means of X-ray diffraction, Vis-UV diffuse reflectance and Raman spectroscopies, nitrogen adsorption at 77 K for determining specific surface areas and surface texture, scanning electron microscopy, and FT-IR monitoring of pyridine adsorption for measuring the surface acidity. Catalytic activity of the samples has been assessed by carrying out as a "probe" reaction the photodegradation of 4-nitrophenol in aqueous medium. The results obtained indicate that incorporation of tungsten on titania leads to formation of different surface species, depending on the tungsten loading. Tungsta microcrystals were detected by X-ray diffraction when the nominal molar W/Ti ratio reached a value of 8.0%. FT-IR investigation indicated that the presence of tungsten induces formation of Brønsted and Lewis surface acid sites. The photoactivity results confirm the beneficial effect of tungsten in TiO_2 for 4-nitrophenol photodegradation in aqueous medium. The reaction rates are higher than those reported in literature for another set of samples and maximum photoactivity was achieved for a sample containing 1.96 moles of W per 100 moles of Ti.

Keywords: 4-nitrophenol photodegradation, WO_x/TiO_2 polycrystalline catalysts, Raman and FT-IR study, Brønsted and Lewis surface acid sites

1. Introduction

Addition of WO_3 to TiO_2 leads to polycrystalline powders used in various heterogeneous catalytic reactions of industrial interest, as for instance alkene isomerization and disproportionation [1–3] and catalytic selective reduction (SCR) of NO by NH_3 [4,5].

In recent years, it has been also observed a beneficial influence of the presence of tungsten oxide in TiO_2 for the occurrence of some photocatalytic processes, such as photo-oxidation of 1,4-dichlorobenzene [6,7] and photodegradation of 4-nitrophenol [8] in aqueous medium. In this latter case the catalysts were prepared by a sol–gel method.

Studies carried out by using different techniques, e.g. X-ray diffraction, XPS, FT-IR spectroscopy, etc., have shown [9] that the preparation method of a powdered catalyst influences the structure of the supported phase and the surface physico-chemical properties of the particles. Consequently, the observed (photo)catalytic activities can be related not only to the intrinsic electronic features of the catalysts, but also to their structural and surface physico-chemical properties [9,10], as determined by the preparation method.

In this paper a study on titania-supported tungsta catalysts prepared by wet impregnation method and with various tungsten loading is reported, aiming mainly at comparing some of their properties and their photoactivities with those showed by similar catalysts prepared by sol–gel method [8].

The powders were characterized by X-ray diffraction (XRD), Vis-UV diffuse reflectance (DRS) and Raman (RS) spectroscopies, nitrogen adsorption at 77 K for determining the specific surface areas and investigating the surface texture, scanning electron microscopy (SEM) and Fourier transform infrared spectroscopy (FT-IR) monitoring of pyridine adsorption for measuring the surface acidity. Moreover, the samples were tested as catalysts for the photodegradation of 4-nitrophenol carried out in aqueous medium.

2. Experimental

2.1. Catalysts preparation

Samples were prepared by the wet impregnation method. The titania support (P-25 from Degussa, Germany; 85% anatase, 15% rutile, $S_{BET} = 53\ m^2\ g^{-1}$) was calcined overnight at 723 K to remove adsorbed organic residues. The solid was subsequently impregnated by using an aqueous solution of ammonium (para)tungstate, $(NH_4)_{10}H_2(W_2O_7)_6$, from Fluka (Germany) and the solvent evaporated until dryness.

* To whom correspondence should be addressed.

The amounts of support and solution were chosen to yield solids containing nominal atomic W/Ti ratios ranging from 0.39 to 12%. The solids were dried in air in an oven at 373 K for 18 h, manually ground in an agate mortar and calcined in air at 723 K for 4 h. Naming of the samples is summarized in table 1, and corresponds to W/Ti/X, where X stands for the round closest value to the atomic W/100Ti ratio.

2.2. X-ray diffraction

X-ray diffraction (XRD) profiles were recorded in a Siemens D-500 instrument, using Ni-filtered Cu $K_{\alpha 1}$ radiation ($\lambda = 154.05$ pm) interfaced to a DACO-MP data acquisition microprocessor equipped with Diffract/AT software.

2.3. Surface area determination and porosity

Specific surface areas (BET) for all of the samples were measured by using a Flowsorb 2300 apparatus (Micromeritics) following the single-point BET method [11]. Cranston and Inkley (S_C) and external (S_t) surface areas for selected samples were determined by studying the full adsorption–desorption isotherms at 77 K in a conventional high-vacuum Pyrex system (residual pressure 10^{-4} N m^{-2}), pressure changes being monitored with a MKS pressure transducer. A porosity assessment of all of the samples was carried out with the same above instrumentation.

2.4. Vis-UV diffuse reflectance spectroscopy

Visible-ultraviolet spectra were recorded by the diffuse reflectance technique using a Shimadzu UV-240 instrument, with MgO or unloaded TiO_2 as a reference and a slit of 5 nm.

2.5. Raman spectroscopy

Raman spectra in the 200–1200 cm^{-1} range were recorded on a computer-controlled Jobin Yvon spectrometer, mod. U-1000, using the 514.5 nm line from a Spectra Physics model 165 Ar^+ laser as the exciting source; the spectral shift-width was typically 5 cm^{-1}, and laser source powers of ca. 400 mW, measured at the sample, were used.

Table 1
Summary of tungsten content, specific BET (S_{BET}), Cranston and Inkley (S_C), external (S_t) surface areas and catalytic activity of the support and W/Ti samples for 4-nitrophenol photo-oxidation

Catalyst	W/Ti [a]	S_{BET} [b]	S_C [b]	S_t [b]	$k_{obs} \times 10^4$ [c]
TiO_2 P-25	–	53	58	53	3.0
W/Ti/0.4	0.39	45	n.m.	n.m.	2.5
W/Ti/1.2	1.17	45	n.m.	n.m.	4.7
W/Ti/2	1.96	44	n.m.	n.m.	6.1
W/Ti/4	3.92	42	44	42	5.2
W/Ti/8	7.83	39	39	38	3.6
W/Ti/12	12.45	35	n.m.	n.m.	3.4

[a] Atoms W/100 atoms Ti.
[b] $m^2 g^{-1}$. n.m. = not measured.
[c] Pseudo-first-order rate constant (s^{-1}).

2.6. FT-IR spectroscopy for surface acidity

Adsorption of pyridine for surface acidity measurements was monitored by FT-IR spectroscopy, using a Perkin-Elmer 16PC spectrometer, connected to an Ataio 386-SX computer, using special cells with CaF_2 windows. Samples were subjected to a conditioning treatment in situ, consisting in outgassing at 673 K for 2 h (residual pressure 10^{-3} N m^{-2}) before performing the adsorption studies.

2.7. Scanning electron microscopy

SEM analyses were performed using a model 505 Philips microscope, operating at 25 kV on specimens upon which a thin layer of gold had been evaporated.

2.8. Photocatalytic experiments

Photoreactivity runs were performed using a 0.5 ℓ Pyrex batch photoreactor. A 125 W medium pressure mercury lamp (Helios Italquartz, B-type) was axially fixed inside the reactor. The photon flux emitted by the lamp was $\Phi_i = 13.5$ mW cm^{-2}. It was measured by using a radiometer UVX Digital leaned against the external wall of the photoreactor containing only pure water.

Oxygen was continuously bubbled into the suspensions for 0.5 h before switching on the lamp and for the duration of the experiments. The catalyst amount and the 4-nitrophenol concentration used were ca. 2 g ℓ^{-1} and $\sim$ 50 mg ℓ^{-1}, respectively. The initial pH of the suspensions was adjusted to 4.5 by addition of H_2SO_4 (Carlo Erba RPE) and the temperature inside the reactor was about 300 K. The photoreactivity runs extended along 3 to 7 h. Samples of 5 ml volume were withdrawn from the suspensions every 10 or 30 min and the catalysts were separated from the solution by filtration through 0.45 μm cellulose acetate membranes (HA, Millipore).

The quantitative determination of 4-nitrophenol was performed by measuring its absorption at 315 nm with a spectrophotometer Varian DMS 90. For the TOC determination a Carlo Erba TCM 480 apparatus was used.

3. Results and discussion

3.1. X-ray diffraction

X-ray diffraction diagrams of the support and of selected samples are shown in figure 1. The support con-

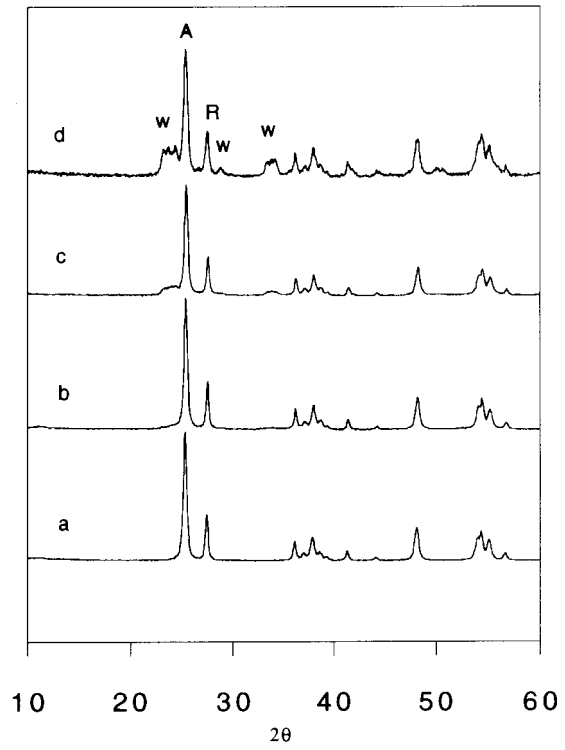

Figure 1. X-ray diffraction diagrams for (a) support TiO_2 P25, (b) sample W/Ti/4, (c) sample W/Ti/8, and (d) W/Ti/12. W = peaks due to WO_3.

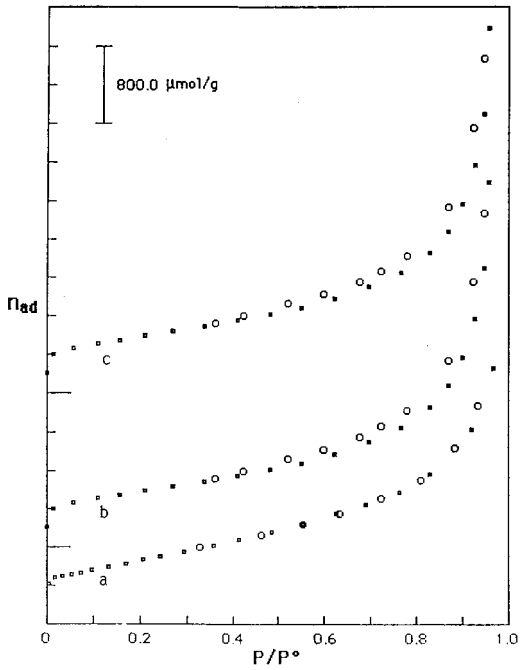

Figure 2. Nitrogen adsorption–desorption isotherms at 77 K on (a) support TiO_2 P25, (b) sample W/Ti/4, and (c) sample W/Ti/8. Small circles: adsorption data; large circles: desorption data. The curves have been vertically displaced for clarity.

sists of both crystallographic phases of titanium dioxide, rutile and anatase [12]. The anatase content is ca. 85% and was determined from the relative intensities of the main diffraction peaks relative to (101) and (110) planes of anatase and rutile, respectively. The diagrams for the low-loaded samples (W/100Ti < 8) are almost coincident with that of the support, with no diffraction peak due to tungsten-containing species, thus suggesting that the tungsten-containing phases are well dispersed on the support surface. The richer W samples, on the contrary, show XRD diagrams where in addition to the peaks of the support, weak peaks at 384 and 265 pm, corresponding to triclinic WO_3 phase, can be observed and the intensities of these peaks increase as the W content does.

3.2. Specific surface area determination and porosity assessment

Nitrogen adsorption–desorption isotherms at 77 K on support and selected samples are shown in figure 2. The isotherm for the support is reversible in the whole relative pressure range, and corresponds to type II in the IUPAC classification [13]. The same type of isotherm is displayed by samples W/Ti/4 and W/Ti/8, although the adsorption capacity somewhat decreases and a small hysteresis loop is observed in the 0.5–0.9 relative pressure range. This hysteresis loop corresponds to type H3 in the IUPAC classification, characteristic of mesoporous samples.

The specific surface areas, as calculated following the BET method, S_{BET}, are reported in table 1 and it can be noticed that they decrease by increasing the tungsten loading.

The cumulative surface areas, S_C, calculated according to the method by Cranston and Inkley [14] are also included in table 1, and coincide with the S_{BET} values, within experimental error, thus confirming the lack of micropores in these samples.

The *t*-plots, not shown for the sake of brevity, fit straight lines passing through the origin, thus definitively confirming the lack of microporosity. The external surface areas, S_t, calculated from the slope to the straight line, also coincide with the S_{BET} values, although for samples W/Ti/4 and W/Ti/8 an upwards deviation of the *t*-plot at high relative pressures, due to adsorption in wide pores [15], can be observed.

Pore-size distribution plots in figure 3 show that pores with a diameter ranging between 2 and 4 nm predominate in the support, while for W/Ti samples the pore diameter range is wider, extending from 2 to 6 nm.

3.3. Vis-UV diffuse reflectance spectroscopy

Vis-UV spectra of the support and W/Ti/4, recorded by the diffuse reflectance technique, are reported in figure 4. MgO or P25 Degussa TiO_2 were used as reference samples.

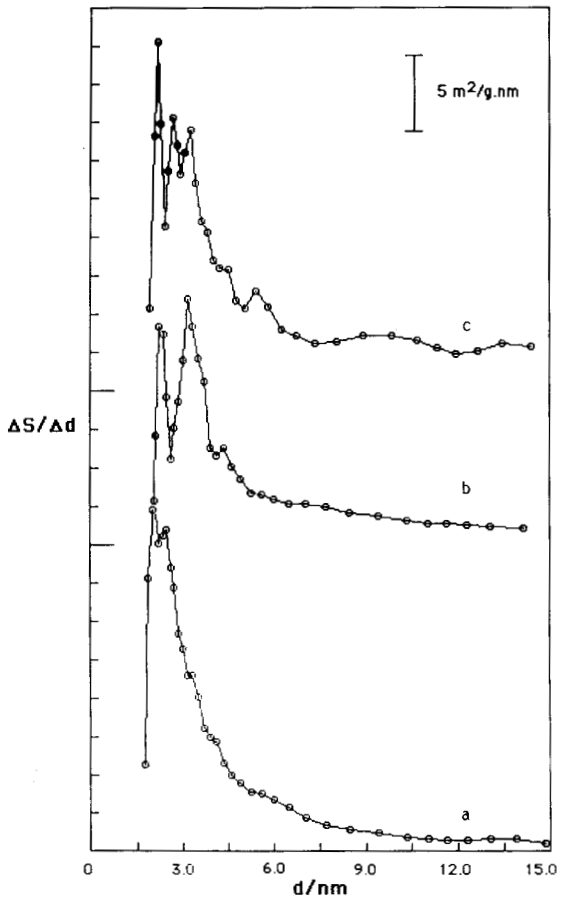

Figure 3. Pore size distribution curves for (a) support TiO_2 P25, (b) sample W/Ti/4, and (c) sample W/Ti/8.

When MgO is used as a reference sample, the spectrum of the support consists of a single, broad, asymmetric and intense absorption from ca. 400 nm to lower wavelengths, usually ascribed to a charge-transfer process from the valence band (mainly formed by 2p orbitals of the oxide anions), to the conduction band (mainly formed by 3d t_{2g} orbitals of the Ti^{4+} cations) [16] and the W/Ti samples show an absorption band similar to that recorded for the support.

When P25 Degussa TiO_2 is used as a reference (the charge-transfer band due to the support is subtracted) a weaker absorption band, with a maximum close to 380 nm is recorded for all W/Ti samples. The intensity of this band, ascribed [17] to a charge transfer process from oxide orbitals to W^{6+} orbitals, increases as the tungsten content does.

3.4. Raman spectroscopy

The Raman spectra of selected samples are shown in figure 5. The support shows bands at 790, 639, 517, and 398 cm^{-1} attributable to anatase, and at 476 cm^{-1} attributable to rutile [18]. When tungsten is present, with contents lower than those required to form the monolayer according to XRD data ($<$ 8 W per 100 Ti atoms; see section 3.1), an additional, weak, broad band is recorded at 964 cm^{-1}. By increasing the tungsten content, the band due to tungsten species slightly shifts towards higher wavenumbers, i.e. at 975 cm^{-1} for sample W/Ti/4 and at 980 cm^{-1} for samples W/Ti/8 and W/Ti/12. This band can be attributed to the W=O stretching mode of surface dispersed bidimensional tungsten oxide species [19].

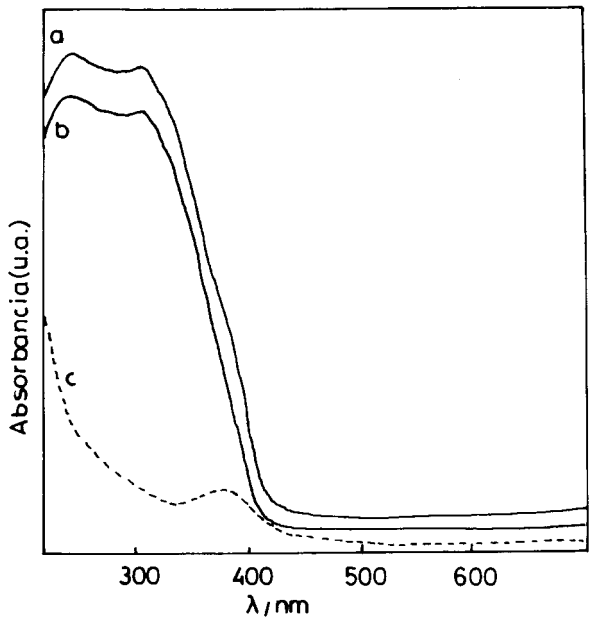

Figure 4. Vis-UV/DR spectra of (a) support TiO_2 P25, (b) and (c) sample W/Ti/4. Reference: solid line MgO; dotted line: parent TiO_2.

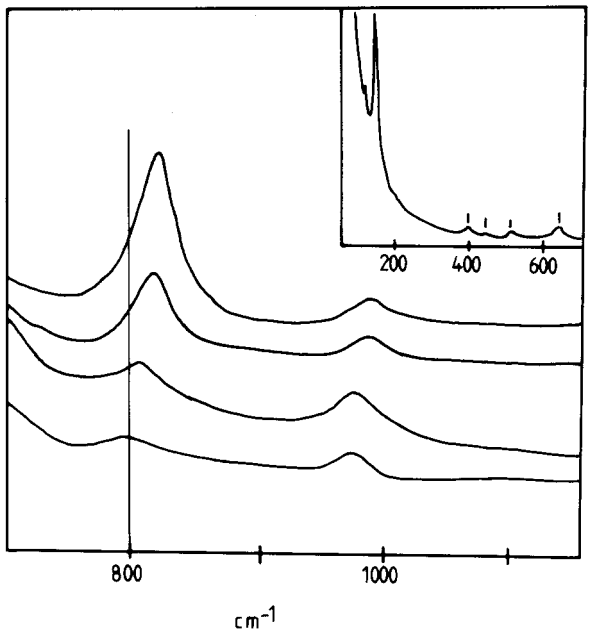

Figure 5. Raman spectra of sample (a) W/Ti/2, (b) W/Ti/4, (c) W/Ti/8 and (d) W/Ti/12. Inset: low $\Delta\nu$ range for sample W/Ti/2.

The fact that only one band is detected indicates the presence of mono-oxo species, because two bands, corresponding to the antisymmetric and symmetric modes, would be recorded [20], if di-oxo species were present. Several authors [20–23] have reported the presence of a single band between 936 and 965 cm^{-1}, which shifts to higher wavenumbers (1010 cm^{-1}) when the spectrum is recorded in situ by using dehydrated samples. These authors ascribe this band to single $[WO_4]$ and/or $[WO_6]$ species, depending on the tungsten loading. In our case, the position of the band is very close to that reported for solvated polytungstates [24], where tungsten does exist in distorted octahedral co-ordination.

For samples W/Ti/8 and W/Ti/12, with tungsten contents larger than that corresponding to the experimental monolayer loading, in addition to the band close to 1000 cm^{-1}, a stronger band is recorded at 806 cm^{-1}, which can be attributed to crystalline WO_3 [25].

Although this band, indeed, could be ascribed to that recorded at 790 cm^{-1} for the titania support and found also in the spectra of other light-loaded W/Ti samples (the bands are very broad and consequently such an ascription cannot be ignored), it should be stressed that the shape of the band is narrower in the case of the high-loaded tungsten samples and the observed shift (from 790 to 806 cm^{-1}) is higher than the instrumental error. It is worth noticing, moreover, that the variation of the shape and of the position of the band can be also noticed in the spectrum recorded for the sample W/Ti/4.

These results confirm the XRD results indicating that the tungsten oxide monolayer is achieved for tungsten loadings just below that corresponding to sample W/Ti/8, and the "molecular" structure of the tungsten-containing species mostly depends on the tungsten loading.

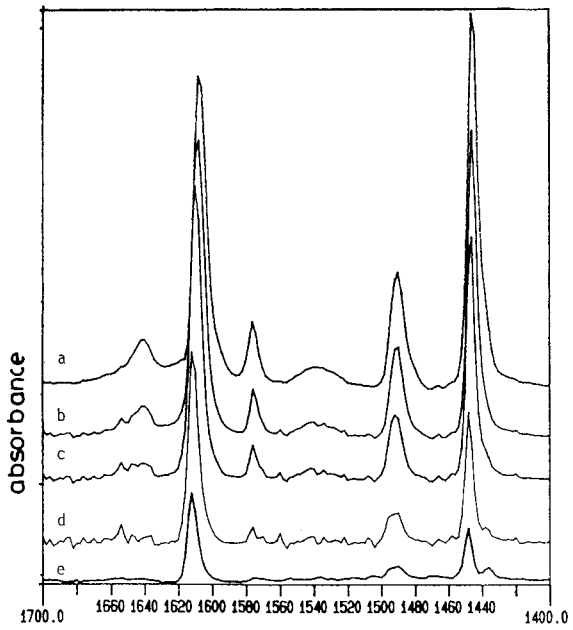

Figure 6. FT-IR spectra recorded after adsorption of pyridine at room temperature on sample W/Ti/2 and outgassing at (a) room temperature, (b) 373, (c) 473, (d) 573, and (e) 673 K.

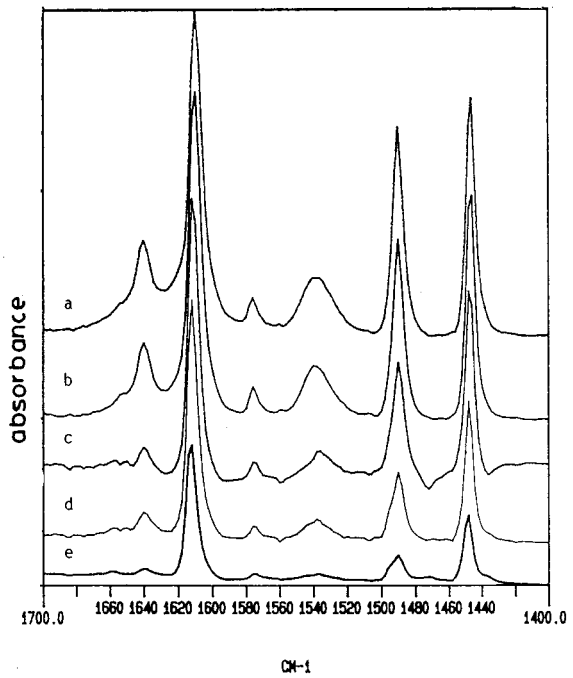

Figure 7. FT-IR spectra recorded after adsorption of pyridine at room temperature on sample W/Ti/8 and outgassing at (a) room temperature, (b) 373, (c) 473, (d) 573, and (e) 673 K.

3.5. *FT-IR spectroscopy for surface acidity*

FT-IR spectra recorded after adsorption of pyridine on samples with different W contents are rather similar. Those corresponding to samples W/Ti/2 (as an example of those samples with low W content) and W/Ti/8 (for those with high W loadings) are shown in figures 6 and 7, respectively. The positions of the bands recorded, as well as their ascription, are given in table 2. The bands at 1607–1610 and 1447 cm^{-1} correspond to modes 8a and

Table 2
Position (cm^{-1}) and ascription of the bands in the FT-IR spectra of pyridine adsorbed on the support and the samples studied

Sample	Bpy [a]			Lpy [b]			
	8a	19a	19b	8a	8b	19a	19b
TiO_2	–	–	–	1604 1592 [c]	1575	1490	1445
W/Ti/0.4	–	–	–	1607	1575	1490	1447
W/Ti/1.2	–	–	–	1607	1575	1490	1447
W/Ti/2	1639	1490	1537	1607	1575	1490	1447
W/Ti/4	1639	1490	1537	1610	1575	1490	1447
W/Ti/8	1639	1489	1539	1610	1577	1489	1447
W/Ti/12	1639	1489	1539	1610	1575	1490	1447

[a] Protonated pyridine bonded to surface Brønsted acid sites.
[b] Pyridine coordinated to surface Lewis acid sites.
[c] Physisorbed pyridine.

19b of pyridine co-ordinated to surface Lewis acid sites, and those recorded at 1537–1539 and 1639 cm^{-1} are characteristic of modes 19b and 8a of protonated pyridine [26]. The presence of these bands indicates that after incorporation of tungsten (even with loadings as low as 2% atoms), surface Brønsted acid sites develop, in addition to surface Lewis acid sites, despite the absence of the former in the support [26,27]. When the tungsten content is increased, the band due to mode 8a of co-ordinated pyridine shifts, and the intensities of the bands due to pyridinium species increase. It can be concluded, consequently, that both surface Lewis and Brønsted acid sites are related to the presence of tungsten species (W^{6+}).

By outgassing at increasing temperatures a steady decrease in the intensities of all bands was observed; however, those due to co-ordinated pyridine remain still

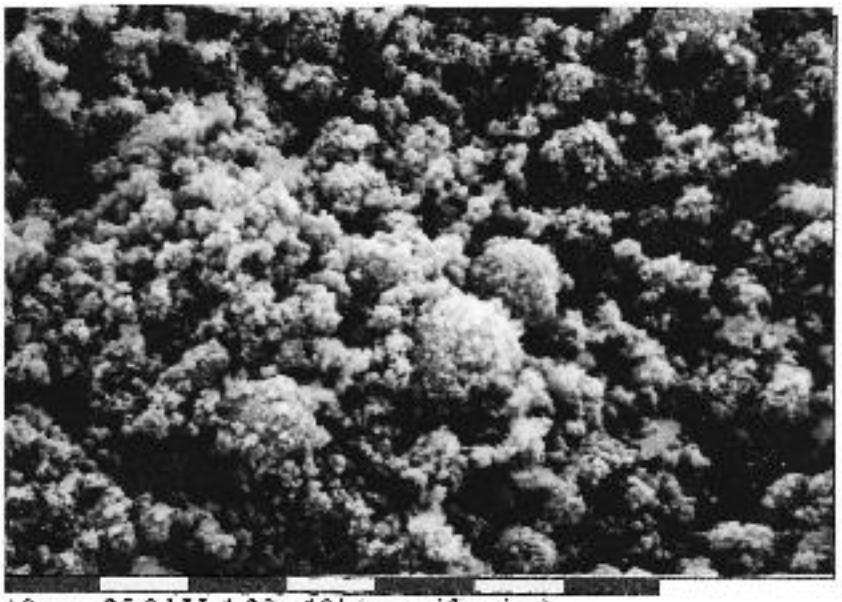

Figure 8. Scanning electron micrographs of (A) pure TiO_2 Degussa P-25; (B) W/Ti/1.2; (C) W/Ti/8; and (D) W/Ti/12. (Continued on next page.)

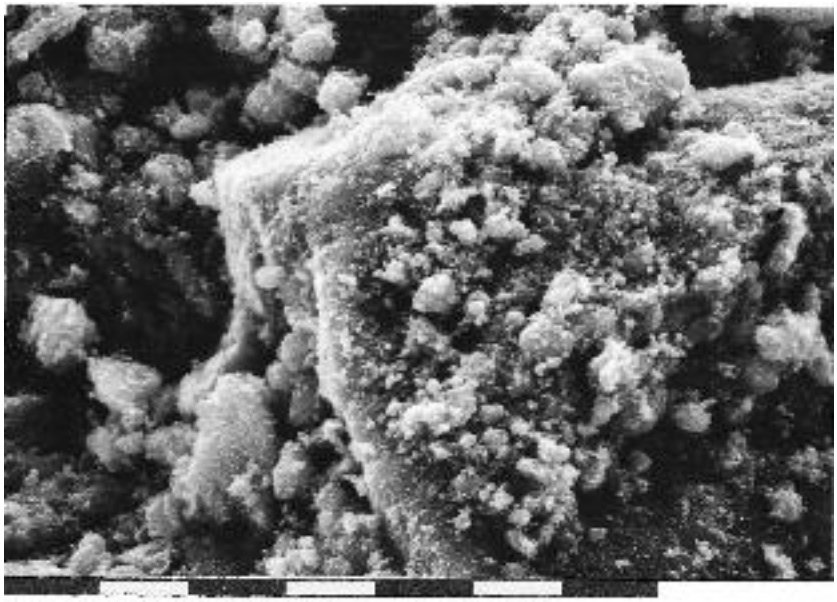

C

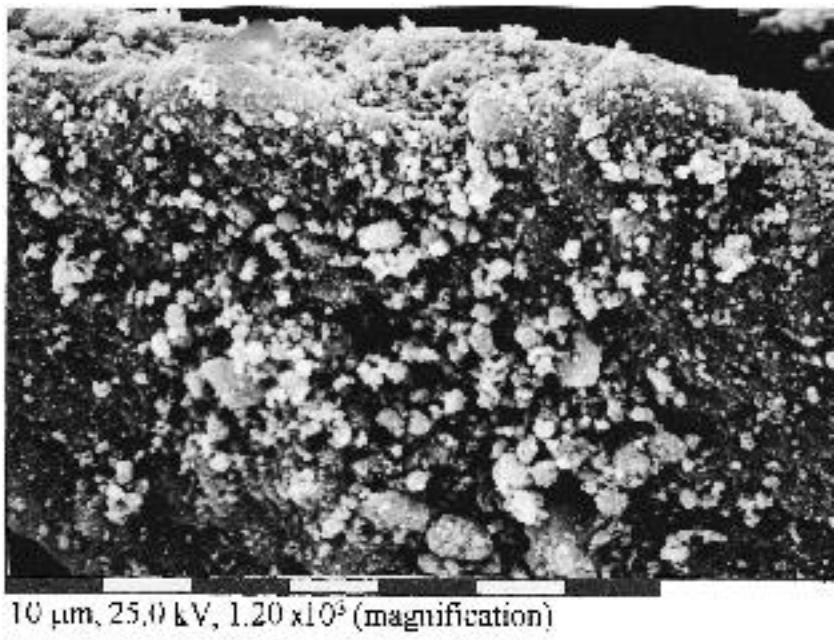

D

Figure 8. (Continued.)

present at higher outgassing temperatures (673 K) than those due to pyridinium species, indicating that the Lewis sites are stronger than the acid ones.

3.6. Scanning electron microscopy

Some selected micrographs of bare TiO_2 and of W/Ti/1.2, W/Ti/8 and W/Ti/12 are shown in figure 8.

No significant morphological differences among the W/Ti samples can be noticed by the observation of the micrographs in figure 8. The shape of the particles for all of the samples is very irregular and some debris attached to the bigger particles are evident. By comparing the W/Ti samples with the bare TiO_2 used as support it can be noticed that the presence of tungsten favors the agglomeration of particles.

3.7. Photocatalytic experiments

The photooxidation of 4-nitrophenol was chosen as a probe reaction [28–30] in order to study the photoactivity of the W/TiO_2 samples and to compare them with the bare TiO_2 used as support and other loaded samples prepared by different methods [6–8].

The photoreactivity results obtained by using the W/Ti samples and the bare TiO_2 sample are reported in table 1 as observed pseudo-first-order rate constant values (k_{obs}). In figure 9 the ratio between 4-nitrophenol concentration and 4-nitrophenol initial concentration versus reaction time is reported for some selected runs. The results indicate that the loaded samples are more photoactive than the corresponding bare TiO_2 with the exception of W/Ti/0.4, of which the photoactivity is slightly lower than that of the support. All the other W/Ti samples showed a photoactivity higher than that of the bare support and among them W/Ti/2 was the most photoactive.

These results are in agreement with the literature [6–8] reporting a beneficial effect of the presence of tungsten in TiO_2 for other sets of W/Ti samples used for photooxidation of organic substrates in aqueous medium. In particular, a set of samples prepared by using the sol–gel method showed a similar trend for the same photoreaction [8] and a maximum of photoreactivity occurred in the presence of a sample containing ca. 1.7 atoms of W per 100 atoms of Ti.

In the set reported in this paper the most active sample, W/Ti/2, contains a tungsten content very close to that of the most photoactive sample prepared by the sol–gel method, but the photoreactivity was ca. an order of magnitude higher [8].

This fact reflects, probably, the intrinsic photoactivity of the corresponding bare TiO_2 used as support and this difference can be understood by taking into account the well known oxidizing capacity of P25 Degussa TiO_2 with respect to other commercial and home-prepared TiO_2 samples [31].

It is well known, on the other hand, that the photoactivity of TiO_2 is strongly influenced by the preparation method [32,33].

The formation of W^{5+} species by means of transfer of photoproduced electrons from TiO_2 to W^{6+} (see section 3.3) can explain the beneficial effect of tungsten on the photoactivity of TiO_2 [7,8].

The lower photoreactivity with respect to bare TiO_2 shown by the lightest loaded sample W/Ti/0.4 can be explained by taking into account that tungsten species could act as recombination centers for the e^-–h^+ pairs recombination according to the following reactions:

$$e^-_{(TiO_2)cb} + W^{6+}_{(bulk)} \rightarrow W^{5+}_{(bulk)} \quad (1)$$

$$h^+_{(TiO_2)vb} + W^{5+}_{(bulk)} \rightarrow W^{6+}_{(bulk)} \quad (2)$$

A detailed discussion on this aspect can be found in ref. [8].

In order to investigate the capacity of the W/Ti impregnated samples to achieve complete photodegradation of 4-nitrophenol, the total organic carbon was analyzed during the runs at fixed time intervals. In figure 10 the ratio between total and initial organic carbon concentration versus reaction time is reported for the bare TiO_2 and some W/Ti sample. It can be observed that the organic carbon disappeared more rapidly (after ca. 3 h instead of ca. 7 h) when the bare TiO_2 was used.

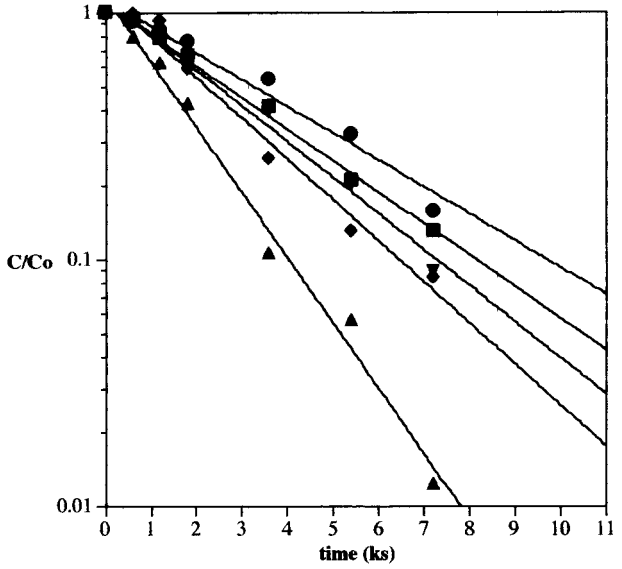

Figure 9. Ratio between 4-nitrophenol concentration at the time t and 4-nitrophenol initial concentration versus illumination time. (■) Bare TiO_2; (●) W/Ti/0.4; (▲) W/Ti/2; (◆) W/Ti/8; and (▼) W/Ti/12.

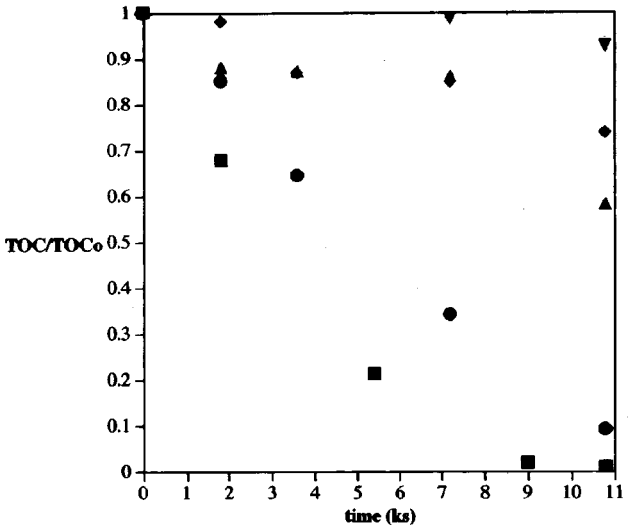

Figure 10. Ratio between total organic carbon concentration (TOC) at the time t and initial total organic carbon concentration (TOC_0) versus illumination time. Symbols as in figure 9.

It is also worth noting that the carbon concentration disappeared more and more slowly by increasing the amount of tungsten of the loaded samples and the formation and accumulation of organic intermediates during the first steps of the photoreaction can explain the delay of disappearance of TOC for some runs shown in figure 10.

FT-IR results indicate the presence of different surface acid–base properties for the support TiO_2 and W/Ti samples.

Although it is difficult to correlate the photoreactivity to each of the several electronic and surface physico-chemical parameters on which it depends, the increasing acidity shown by the W/Ti samples (the higher, the higher the tungsten content) could play a major role in lowering the 4-nitrophenol mineralisation rate observed for these samples with respect to bare TiO_2. The explanation could be found in the less significant interaction between the surface of the catalyst and the 4-nitrophenol and/or the intermediates species produced in the first oxidation steps of the reaction.

It can be concluded that the W/Ti impregnated samples are more photoactive than the corresponding bare TiO_2 when the organic substrate disappearance rate is considered, but with respect to the complete photo-oxidation of 4-nitrophenol, the bare TiO_2 used as support (Degussa P-25) showed to be more photoactive than each of the W/Ti impregnated samples.

For the samples prepared by the sol–gel method [8], the bare TiO_2 was more or less photoactive than the loaded samples, depending on the amount of tungsten. Moreover, the presence of traces of carbon due to the sol–gel preparation method carried out by using tungsten(IV) oxychloride, the different type of pores, the different surface hydroxylation along with many other differences in the physico-chemical surface properties could be responsible for the slower photoactivity of these samples with respect to the impregnated W/Ti ones.

Acknowledgement

Financial support from Ministerio de Educación y Ciencia (Madrid, grant PB93-0633) is appreciated. GS acknowledges a sabbatical leave from Universidad de Guanajuato (Mexico). GM, LP and AS gratefully acknowledge financial support by the Ministero dell'Università e della Ricerca Scientifica e Tecnologica (Rome).

References

[1] M. Ai, J. Catal. 49 (1977) 305.
[2] T. Yamaguchi, Y. Tanaka and K. Tanabe, J. Catal. 65 (1980) 442.
[3] T. Yamaguchi, S. Nakamura and H. Naguno, in: *Proc. 8th Int. Congr. on Catalysis*, Vol. 5 (Verlag Chemie, Weinheim, 1984) p. 579.
[4] M. Imanari, Y. Watanabe, S. Matsuda and F. Nakajima, in: *Proc. 7th Int. Congr. on Catalysis*, eds. T. Seiyama and K. Tanabe (Elsevier, Amsterdam, 1981) p. 841.
[5] S. Morikawa, K. Takahashi, J. Mogi and S. Kurita, Bull. Chem. Soc. Jpn. 55 (1982) 2254.
[6] W. Lee, W.M. Gao, K. Dwight and A. Wold, Mater. Res. Bull. 27 (1992) 685.
[7] Y.R. Do, W. Lee, K. Dwight and A. Wold, J. Solid State Chem. 108 (1994) 198.
[8] G. Marcì, L. Palmisano, A. Sclafani, A.M. Venezia, R. Campostrini, G. Carturan, C. Martín and G. Solana, J. Chem. Soc. Faraday Trans. 92 (1996) 819.
[9] G.A. Somorjai, *Introduction to Surface Chemistry and Catalysis* (Wiley, New York, 1994).
[10] M. Schiavello, Electrochim. Acta 38 (1993) 11.
[11] H. Bosch and E. Peppelenbos, J. Phys. E 10 (1977) 605.
[12] JCPDS files 21-1276, 21-1275.
[13] K.S.W. Sing, D.H. Everett, R.A.W. Haul, L. Moscou, R.A. Pierotti, J. Rouquerol and T. Sieminewska, Pure Appl. Chem. 57 (1985) 603.
[14] R.W. Cranston and F.A. Inkley, Adv. Catal. 9 (1957) 143.
[15] S. Lowell and J.E. Shields, *Powder Surface Area and Porosity* (Chapman & Hall, London, 1984).
[16] E. Borgarello, J. Kiwi, M. Grätzel, I. Pelizzetti and M. Visca, J. Am. Chem. Soc. 104 (1982) 2996.
[17] C.K. Jørgensen, *Absorption Spectra and Chemical Bonding in Complexes* (Pergamon Press, Oxford, 1962).
[18] R.J. Capwell, F. Spagnolo and M.A. Sesa, Appl. Spectrosc. 26 (1972) 537.
[19] G. Deo and I.E. Wachs, J. Phys. Chem. 95 (1991) 5889.
[20] G. Ramis, G. Busca, C. Cristiani, A.S. Elmi and P. Villa, J. Mol. Catal. 61 (1990) 319.
[21] D.S. Kim, M. Ostromecki and I.E. Wachs, J. Mol. Catal. 106 (1996) 93.
[22] S.S. Chan, I.E. Wachs, L.L. Murrell, L. Wang and W.K. Hall, J. Phys. Chem. 88 (1984) 5831.
[23] M.A. Vuurman, I.E. Wachs and A.M. Hit, J. Phys. Chem. 95 (1991) 9928.
[24] C.F. Baes Jr. and R.E. Mesmer, *The Hydrolysis of Cations* (Wiley, New York, 1970).
[25] I.R. Beattie and T.R. Gilson, J. Chem. Soc. (1965) 2322.
[26] H. Miyata, Y. Nakagawa and H. Naguno, J. Chem. Soc. Faraday Trans. I 79 (1983) 2343.
[27] V. Rives, Opt. Pura Apl. 16 (1983) 61.
[28] L. Palmisano, V. Augugliaro, M. Schiavello and A. Sclafani, J. Mol. Catal. 56 (1989) 284.
[29] V. Augugliaro, L. Palmisano, M. Schiavello, A. Sclafani, L. Marchese, G. Martra and F. Miano, Appl. Catal. 69 (1991) 323.
[30] V. Augugliaro, M.J. López-Muñoz, L. Palmisano and J. Soria, Appl. Catal. A 101 (1993) 7.
[31] I. Sopyan, M. Watanabe, S. Murasawa, K. Hashimoto and A. Fujishima, J. Photochem. Photobiol. A 98 (1996) 79.
[32] A. Sclafani, L. Palmisano and M. Schiavello, J. Phys. Chem. 94 (1990) 829.
[33] A.P. Rivera, K. Tanaka and T. Hisanaga, Appl. Catal. B 3 (1993) 37.